physica status solidi rrl
www.pss-rapid.com

Ferroelectric La-Doped $ZrO_2/Hf_xZr_{1-x}O_2$ Bilayer Stacks with Enhanced Endurance

Mihaela Popovici, Amey M. Walke, Kaustuv Banerjee, Nicolo Ronchi, Johan Meersschaut, Umberto Celano, Sean McMitchell, Valentina Spampinato, Alexis Franquet, Paola Favia, Johan Swerts, Geert Van den Bosch, and Jan Van Houdt**

Hafnium zirconate (HZO) is investigated in metal–ferroelectric–metal capacitors as a function of Hf/(Hf+ Zr) atomic ratio, the presence of a thin ZrO_2 seed layer, and/or by doping HZO with La^{3+}. It is demonstrated that a longer endurance is achieved with Hf-rich HZO by introducing a ZrO_2 seed layer. The endurance is further improved by introducing La^{3+} in the Hf-rich HZO layer of the bilayer stack, which offers a higher $2P_r$ in the pristine state compared with a stoichiometric HZO doped with the same amount of La^{3+}. Both ZrO_2 underlayer and La^{3+} doping of HZO are shown to play a decisive role in promoting the formation of an orthorhombic and tetragonal phase at the expense of a detrimental monoclinic phase.

1. Introduction

For next-generation ferroelectric random-access memory (FERAM), high-endurance (above 10^{12} cycles) metal–ferroelectric–metal capacitors (MFMs) are required, where both the ferroelectric and the metal have to be deposited by highly conformal techniques such as atomic layer deposition (ALD). The twin oxides HfO_2 and ZrO_2 have the advantage of forming hafnium zirconate (HZO) solid solutions, where the ferroelectric behavior is maintained in HZO ($Hf_xZr_{1-x}O_2$) in a wide range of compositions.[1,2] It is generally accepted that stoichiometric ($x = 0.5$) hafnium zirconate (50% Hf–50% Zr) shows the best ferroelectric behavior for a given set of experimental conditions (precursors, deposition temperature, electrodes, annealing parameters).[3] Moreover, doping with La^{3+} was shown to increase the endurance with more than one order of magnitude as compared with pure stoichiometric HZO.[4,5] Ferroelectricity originates from noncentrosymmetric orthorhombic *Pca21* phase, which can be stabilized by strain, grain size, and dopant concentration. To increase the endurance, the stability of orthorhombic phase has to be enhanced, whereas the formation of monoclinic phase, mainly responsible for the fatigue behavior,[6] has to be avoided as much as possible, while maintaining the remanent polarization ($2P_r$) at conveniently high values.[5] In this respect, the grain size should be small enough to prevent the formation of a thermodynamically stable monoclinic phase. Several studies were dedicated to improve the ferroelectric behavior of HZO deposited at Hf:Zr = 1:1 ratio using (Hf/Zr)[$N(C_2H_5)CH_3]_4$ precursor with a final Zr:Hf = 0.43:0.57 ratio, via a nucleation layer such as HfO_2, Al_2O_3, or ZrO_2.[7–9] Improved ferroelectric properties were obtained with a 2 nm-thick ZrO_2[8,9] for HZO film thickness varying between 10 and 25 nm.[7–10] In this study, we evaluate the effect of adding a nucleation layer, such as ZrO_2, with variable thickness (1–2 nm), the Hf/Zr ratio, and the La^{3+} doping level on the ferroelectric characteristics of hafnium zirconate with physical thickness ≤10 nm.

2. Results and Discussion

The as-grown films were partially crystallized, as indicated by GIXRD in **Figure 1**a (gray line pattern). However, the Hf-rich HZO ($Hf_{0.57}Zr_{0.43}O_2$) showed delayed crystallization as compared with stoichiometric ($Hf_{0.50}Zr_{0.50}O_2$) or Zr-rich HZO ($Hf_{0.43}Zr_{0.57}O_2$), as indicated by lower-intensity peak at $2\theta \approx 30.5°$. After postmetallization anneal, the main peak intensity (black line pattern in Figure 1a) was comparable, indicating complete crystallization of all HZO films. SEM top-view images of the as-grown films confirmed that lower density of nanocrystallites was present in the Hf-rich HZO as compared with stoichiometric HZO, whereas the Zr-rich HZO showed the largest density of grains (**Figure 2**). Therefore, after postmetallization anneal, we expect larger grains to be present in the Hf-rich

Dr. M. Popovici, Dr. A. M. Walke, Dr. K. Banerjee, Dr. N. Ronchi, Dr. J. Meersschaut, Dr. U. Celano, Dr. S. McMitchell, Dr. V. Spampinato, Dr. A. Franquet, Dr. P. Favia, Dr. J. Swerts, Dr. G. Van den Bosch, Dr. J. Van Houdt
STS
IMEC
Kapeldreef 75, Leuven 3001, Belgium
E-mail: Mihaela.Ioana.Popovici@imec.be; Jan.VanHoudt@imec.be

Dr. U. Celano
Faculty of Science and Technology
University of Twente
P.O. Box 217, 7500 AE Enschede, The Netherlands

Dr. J. Van Houdt
Semiconductor Physics
Physics and Astronomy – KU Leuven
Celestijnenlaan 200d - box 2417, 3001 Leuven, Belgium

The ORCID identification number(s) for the author(s) of this article can be found under https://doi.org/10.1002/pssr.202100033.

DOI: 10.1002/pssr.202100033

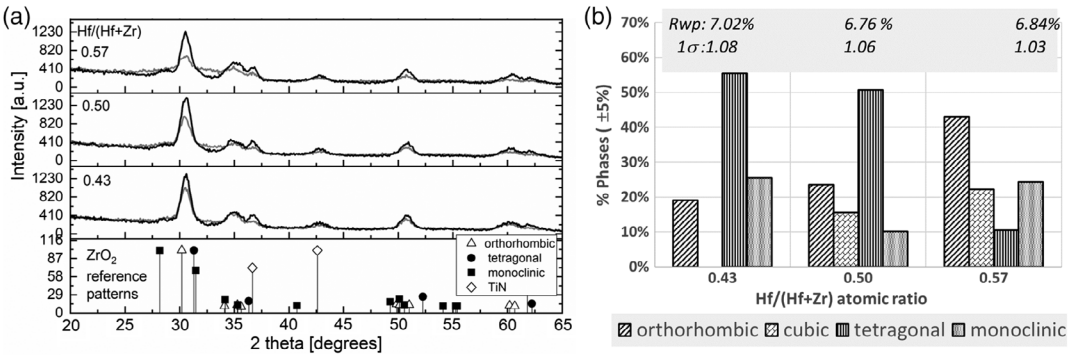

Figure 1. a) GIXRD patterns, b) Hf-rich HZO (dotted experimental data vs fit red line), and c) phase content as a function of Hf/(Hf + Zr) atomic ratio (Rwp% and 1σ parameters describing the quality of refinements are given for each set of data fit).

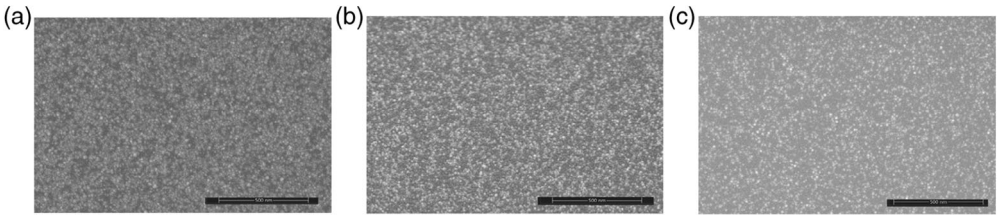

Figure 2. a–c) SEM top view of the as-grown $Hf_{0.43}Zr_{0.57}O_2$ films (a), $Hf_{0.50}Zr_{0.50}O_2$ (b), and $Hf_{0.57}Zr_{0.43}O_2$ (c).

HZO films due to the lower amount of nuclei formed at the deposition stage, whereas Zr-rich HZO would keep the small grain size. Therefore, it is likely that the orthorhombic domain size would depend on the initial grain size. Apart from changing the grain size, structural modifications induced by different ionic sizes of Hf^{4+} and Zr^{4+} with Hf/Zr ratio could have an essential impact on the phase content formed in the fully crystallized films. By Rietveld refinement of the diffraction spectra conducted using the Material Analysis Using Diffraction (Maud) software,[11] in combination with crystallographic information files for monoclinic, orthorhombic, tetragonal, and cubic phases of ZrO_2 and cubic TiN, we quantified the relative amount of HZO phases present in the TiN–HZO–TiN stacks (Figure 1b). The Maud software uses the Rietveld algorithm to optimize the model function by minimizing the weighted sum of squared differences between the experimental and computed intensity values. The quality of the refinements for each diffraction spectra is expressed by the weighted profile *R*-factor "Rwp," along with 1σ (Figure 1b). This method of phase quantification was also used by Mukundan et al.[12] in 10 nm stoichiometric HZO.

In the case of Zr-rich HZO, the tetragonal phase was predominant, and this phase content diminished with the increase in Hf content, whereas the orthorhombic phase increased with Hf content. About 43% of the orthorhombic phase was obtained for $Hf_{0.57}Zr_{0.43}O_2$ films in the pristine state, in agreement with the largest initial polarization in this case (**Figure 3**).

The polarization–electric field (*P*–*E*) loops in the pristine state are more pinched for the Zr-rich HZO (**Figure 4**a). The multiple-switching current peaks seen in the current-applied field and corresponding to the pinched loop in Zr-rich layers, which were also observed in ZrO_2 or other Zr-rich HZO films,[13] were attributed to the presence of a large amount of tetragonal phases. Through

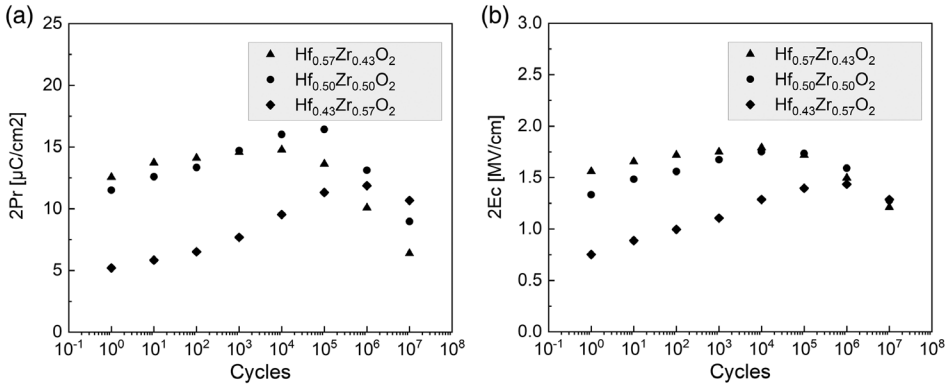

Figure 3. a) $2P_r$ and b) $2E_c$ when *P*–*V* measurements are carried out with an amplitude of 2 MV cm^{-1} as a function of the number of bipolar cycles at a frequency of 250 kHz.

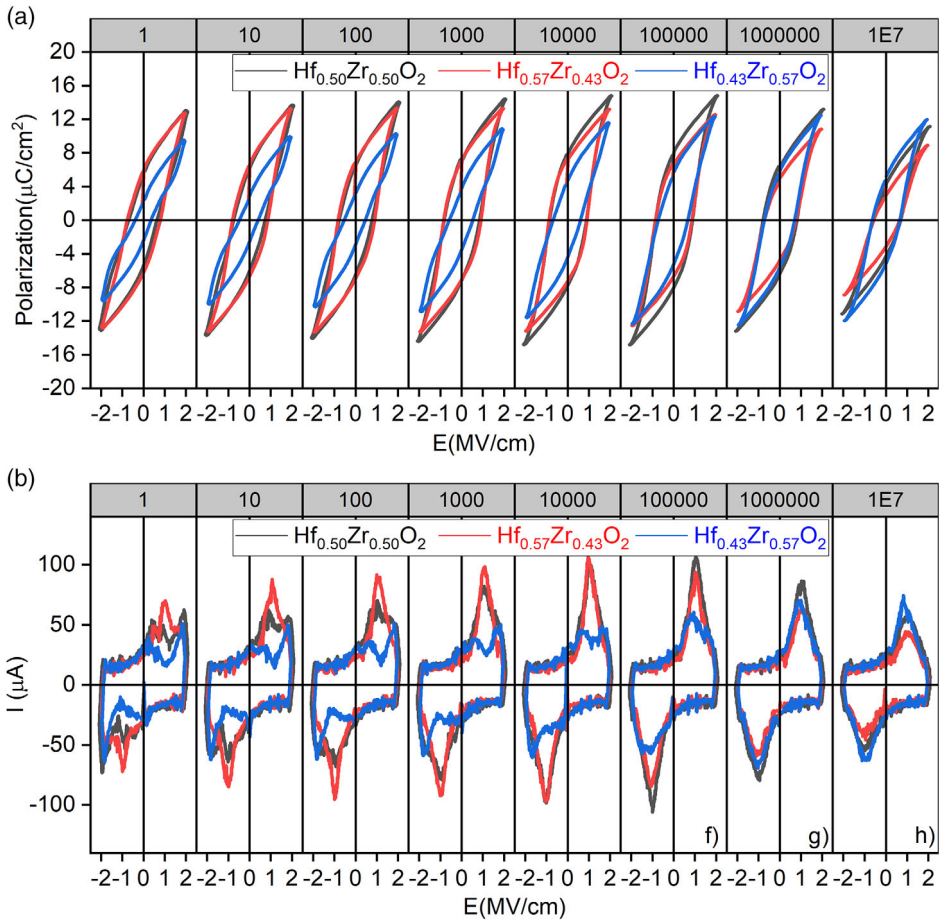

Figure 4. a) *P–E* and b) *I–E* hysteresis curves variation with the applied field cycles on $Hf_xZr_{1-x}O_2$.

further cycling required for loops' opening, the switching current peaks merge, as shown in Figure 4b. With increase in Hf content, current peaks merge and an open *P–V* loop response is seen.

Figure 3 and 4 allowed the assessment of cycling performance of Hf-rich, stoichiometric, and Zr-rich HZO films. As expected, Hf-rich and stoichiometric HZO films exhibited a higher initial $2P_r$ in accordance with high orthorhombic phase content observed in the pristine state. The larger polarization for Hf-rich HZO is in agreement with the previous report of Park et al.[1] **Table 1** shows a comparison of wake-up (difference between maximum and initial $2P_r$) as a function of Hf/(Hf + Zr) ratio.

Table 1. Wake-up effect as a function of Hf/(Hf+Zr) atomic ratio.

Hf/(Hf + Zr)[a)]	Initial $2P_r$ [μC cm^{-2}][b)]	Maximum $2P_r$ [μC cm^{-2}]	$\Delta 2P_r$ [μC cm^{-2}][c)]	Onset of Fatigue
0.57	12.4	14.7	2.3	$>10^4$
0.50	10.8	16.4	5.6	$>10^5$
0.43	5.4	11.8	6.4	$>10^6$

[a)]Atomic ratio; [b)]Initial $2P_r$ when *P–V* measurements are carried out with an amplitude of 2 MV cm^{-1}; [c)]$\Delta 2P_r$ = maximum $2P_r$ − initial $2P_r$).

A prolonged wake-up is seen for Zr-rich films, which have low orthorhombic phase content and high tetragonal phase content in the pristine state. Figure 3 also shows that the onset of fatigue is also a function of initial orthorhombic content. It could be seen that the Hf-rich layer with the highest orthorhombic content shows earliest start of fatigue (above 10^4 cycles) in agreement with previous reports,[1,2,13] followed by stoichiometric (above 10^5 cycles) and Zr-rich layer (above 10^6 cycles). This evolution could be attributed to increase in the domain size of orthorhombic phase, and further phase conversion into thermodynamically stable monoclinic phase,[6] likely due to a larger driving force for this phase transition, which appears at larger size. One can expect that the domain size of the orthorhombic phase increases through cycling. By surpassing a critical grain size threshold, the transition into monoclinic phase, mainly responsible for fatigue, could occur. The reason for orthorhombic domain size enlargement can be related to the conversion of tetragonal phase,[14] residing at the interfaces as suggested by Künneth et al.,[15] to orthorhombic phase and consequently the path for further coalescence of orthorhombic domains into larger ones was favored.

In principle, the domain coalescence phenomenon is favorable for polarization enhancement and could be one of the mechanisms responsible for increase in polarization. Nevertheless, other concurrent mechanisms, such as the conversion of the

nonpolar orthorhombic into polar orthorhombic phase, nonuniform distribution of charged defects (e.g., oxygen vacancies), depinning of domains, and alignment of their polarization along the applied electrical field, are not excluded.[16–21] As shown in Figure 3b, the coercive field ($2E_c$) seems to increase with the number of applied field cycles, which is related to the opening of *P*–*E* loops, as shown in Figure 4.

Based on the results above, we observed that Hf-rich HZO improves $2P_r$ in the pristine state but shows earlier fatigue in agreement with a stronger thermodynamic driving force for monoclinic phase formation,[2] whereas Zr-rich HZO offers better endurance. In the follow-up experiment, we tried to improve the endurance of Hf-rich HZO, using a bilayer stack structure, in which Hf-rich HZO was grown on a ZrO_2 seed layer. The 1 or 2 nm-thick ZrO_2 layer was inserted at the interface between the TiN bottom electrode and Hf-rich HZO, with and without La^{3+} doping (1.6 at% La). The ZrO_2 seed layer was used with the purpose of favoring the formation of the smaller orthorhombic domain size into the Hf-rich HZO top layer and, consequently, to delay conversion of orthorhombic phase to monoclinic phase and therefore improving the endurance.

Quantification of the phases present in the bilayer stacks in the pristine state (**Figure 5**) showed a decrease in orthorhombic phase, concomitantly with the gradual increase of tetragonal phase content. The same trend was observed with the increase in the thickness of ZrO_2 underlayer and when adding La^{3+} as a dopant. The tetragonal phase became the predominant phase for the 2 nm ZrO_2/La: $Hf_{0.57}Zr_{0.43}O_2$, for which the monoclinic phase content was the lowest.

To compare the ferroelectric behavior of the bilayer stacks with longer endurance cycles (up to 10^{10} cycles), we included in our study a reference layer, e.g., a La-doped stoichiometric HZO (La: $Hf_{0.50}Zr_{0.50}O_2$)-based stack. No monoclinic phase was seen in La-doped stoichiometric HZO, similar to the study by Kozodaev et al.,[5] even though its presence cannot be completely ruled out. However, Rietveld refinement showed only a mixture of orthorhombic (54%) and tetragonal (40%) phases, next to a small amount of cubic phase (6%). At the same Hf/Zr ratio, not only the method of fabrication,[21] the precursors used, the deposition temperature, and the crystallization temperature, but also the La dopant concentration[5,22] will affect the relative ratio of the phases and consequently the ferroelectric response (e.g., polarization, endurance, and retention).[23] Rietveld refinement shows an increased amount of orthorhombic phase with introduction of La dopant in stoichiometric HZO, while reducing the cubic and monoclinic phase.

We examined the chemical depth profile of elements present in the corresponding $ZrO_2/Hf_{0.57}Zr_{0.43}O_2$ and ZrO_2/La: $Hf_{0.57}Zr_{0.43}O_2$ bilayer stacks by TOFSIMS analysis (**Figure 6**a). No intermixing could be evidenced between the two layers after postmetallization anneal, as observed when comparing the Zr^+ and Hf^+ in-depth signal. Moreover, La^+ is localized into HZO; thus, no out-diffusion into ZrO_2 bottom layer was observed. The EDS depth profile of Zr, Hf, and O for the 2 nm ZrO_2/Hf-rich HZO sample confirmed that two distinct layers ZrO_2 and HZO are present in the stack (Figure 6b).

In **Figure 7**, the cycling endurance test was conducted at a field amplitude of 2.5 MV cm^{-1}, with the exception of 1 nm

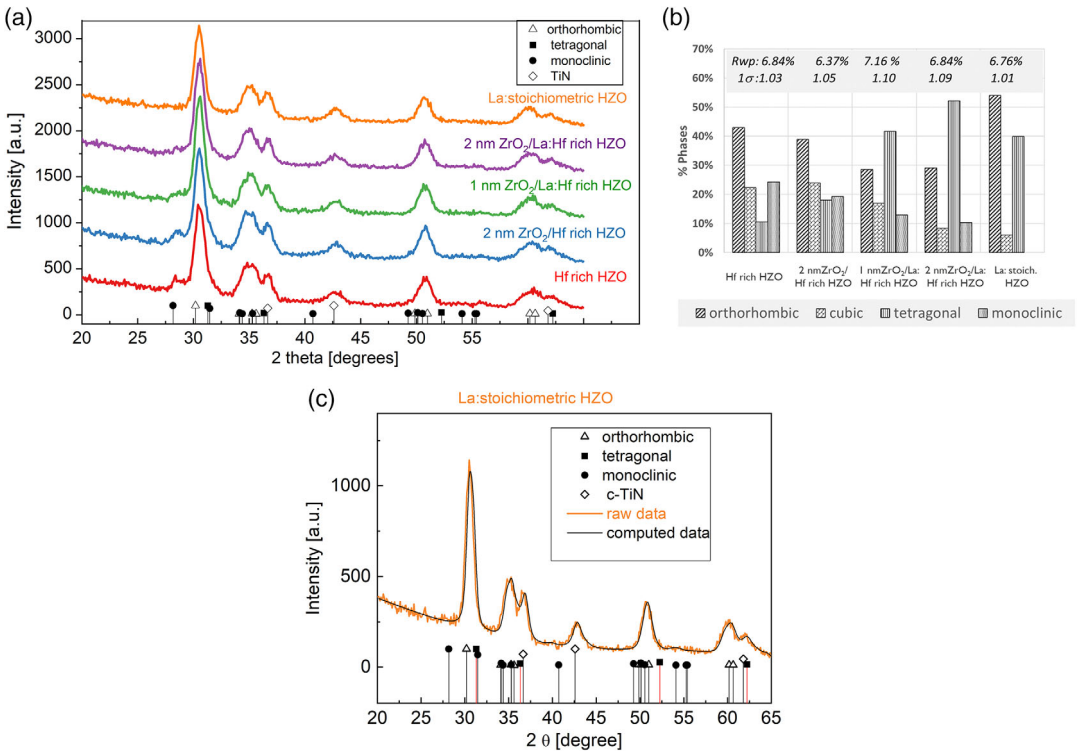

Figure 5. a) GIXRD patterns and b) phase content of Hf-rich HZO, undoped, and La-doped ZrO_2/Hf rich HZO, and La-doped stoichiometric HZO. c) GIXRD pattern, experimental data (beige line), and fit (black line, Rwp = 6.72%, $1\sigma = 1.03$) for La:$H_{f0.50}Zr_{0.50}O_2$.

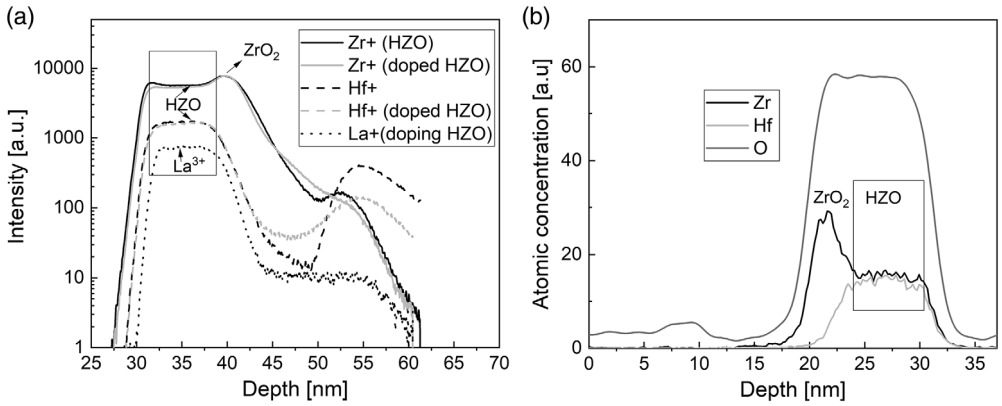

Figure 6. a) TOFSIMS depth profile of 2 nm ZrO_2/Hf-rich HZO and 2 nm ZrO_2/La:Hf-rich HZO. b) EDS depth profile of 2 nm ZrO_2/Hf-rich HZO.

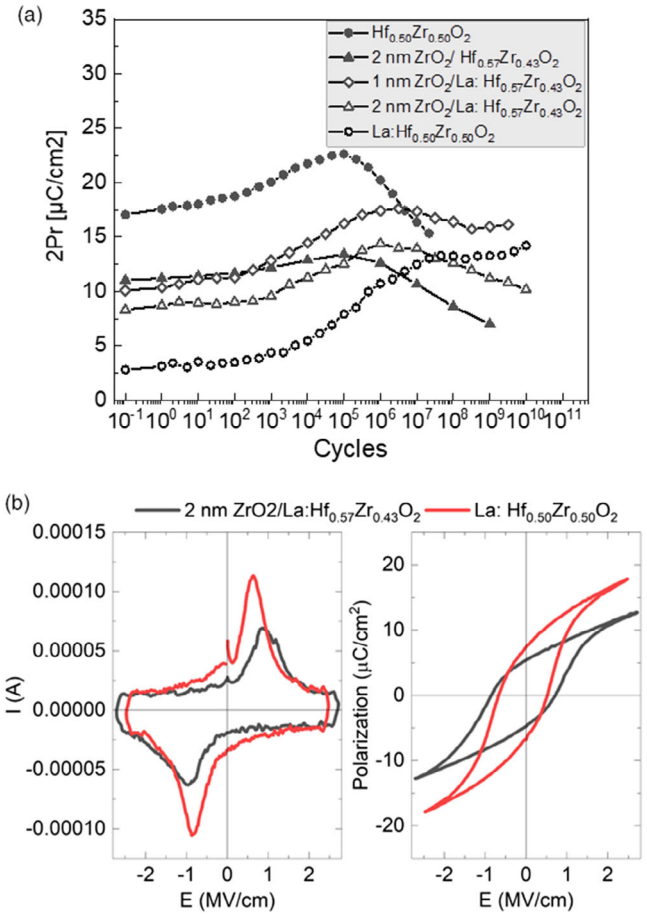

Figure 7. Endurance characteristics of (doped) HZO with and without ZrO_2 seed. Bipolar pulses with rise and fall time of 200 ns were used for fatigue measurements (833 kHZ). a) *I–E* and b) *P–E* hysteresis curves variation with the applied field cycles on 2 nm ZrO_2/La:$Hf_{0.57}Zr_{0.43}O_2$ and La: $Hf_{0.50}Zr_{0.50}O_2$ at 10^{10} switching cycles.

ZrO_2/La: $Hf_{0.57}Zr_{0.43}O_2$, for which the field amplitude was slightly higher (2.8 MV cm^{-1}).

As no intermixing occurred postannealing between ZrO_2 and $Hf_{0.57}Zr_{0.43}O_2$, the ferroelectric response of the bilayer stacks was determined mainly by the Hf-rich HZO layer. $2P_r$ after one cycle was lower (11.2 μC cm^{-2}) for the 2 nm ZrO_2/$Hf_{0.57}Zr_{0.43}O_2$ as compared with stoichiometric HZO. This agrees with the lower orthorhombic phase content in the pristine state. About 1.6 at% La doping further reduces $2P_r$, though it improves endurance of ZrO_2/La: $Hf_{0.57}Zr_{0.43}O_2$. The maximum of $2P_r$ (14.4 μC cm^{-2}) was achieved at 10^6 cycles for the 2 nm ZrO_2/La: $Hf_{0.57}Zr_{0.43}O_2$, which is higher than the maximum $2P_r$ (13.4 μC cm^{-2}) corresponding to the undoped ZrO_2/$Hf_{0.57}Zr_{0.43}O_2$. If the thickness is reduced to 1 nm, $2P_r$ increase is again observed, which can indicate larger domain size of the orthorhombic phase or less pinning of the ferroelectric domains. This could be related to the impact of the island-like ZrO_2, which is not yet a completely closed layer at a thickness of 1 nm. Therefore, the Hf-rich HZO grown on top of 1 nm ZrO_2 could have a direct contact to the TiN bottom electrode in some areas. This could favor a mechanism of nucleation similar to Hf-rich HZO on TiN, as shown in Figure 2, responsible for a larger orthorhombic domain size upon crystallization. In comparison, the initial $2P_r$ of La:$Hf_{0.50}Zr_{0.50}O_2$ was modest (3.1 μC cm^{-2}) and required a long wake-up. After 10^6cycles, $2P_r$ was still inferior (10.7 μC cm^{-2}), as compared with the 2 nm ZrO_2/La: $Hf_{0.57}Zr_{0.43}O_2$ stack, and became comparable only at 10^{10} cycles (14.2 μC cm^{-2}). Moreover, no impact of the leakage can be seen at 10^{10} switching cycles (Figure 7b). Even though the 2 nm ZrO_2/La: $Hf_{0.57}Zr_{0.43}O_2$ stack showed a decrease of $2P_r$ at 10^{10}cycles (10.2 μC cm^{-2}), it demonstrates the benefit of using ZrO_2 seed for a faster wake-up, likely applicable also for stoichiometric HZO.

3. Conclusion

The impact of a ZrO_2 seed layer on the crystallization and ferroelectric behavior of hafnium zirconate (undoped or doped with La^{3+}) was assessed. The content of crystalline phases of polymorphic HZO in pristine state was used to explain the initial polarization and further behavior during the endurance tests. The increase in endurance of the Hf-rich HZO with the addition of ZrO_2 seed and/or the La^{3+} dopant at low concentrations was found to correlate with the reduction of monoclinic phase content. Addition of a 2 nm ZrO_2 seed layer extended endurance of

Hf-rich HZO layer. Moreover, doping of $Hf_{0.57}Zr_{0.43}O_2$ grown on 2 nm ZrO_2 seed layer with La improved the endurance even further to 10^{10} cycles. In the absence of the ZrO_2 seed and the La^{3+} dopant, we observed an accelerated fatigue for Hf-rich HZO, which could be correlated with the presence of higher monoclinic phase content. The seed layer used for growth of the ferroelectric layer was found to be a crucial parameter in controlling the relative phase ratio of polymorphic hafnium zirconate. However, further experiments are needed to understand if the increase in polarization is due to the change in domain size of orthorhombic phase occurring during electric field cycling and/or if the domains align along the applied electrical field. A combination of ZrO_2 interfacial layer with Hf-rich HZO also promoted a faster wake-up behavior. In addition, the La^{3+} was used to further reduce the monoclinic phase content in Hf-rich HZO, thereby improving the endurance, while at the same time offering higher $2P_r$ in the pristine state as compared with La-doped stoichiometric HZO.

4. Experimental Section

HZO films were grown by a thermal ALD process on 10 nm TiN deposited on Si(100) wafers (300 mm diameter) at 300 °C using $HfCl_4$ and $ZrCl_4$ (Versum Materials) as metal sources and H_2O as oxidant, at Hf:Zr pulse ratios of 1:1, 4:3, and 3:4. The Hf/(Hf + Zr) atomic ratios obtained were 0.50, 0.57, and 0.43, respectively. Prior to ≈10 nm-thick HZO deposition, a 1 nm or a 2 nm ZrO_2 seed layer was deposited in some cases. Lola' (Air Liquide) was used as precursor for La^{3+} doping. A 10 nm TiN cap layer was deposited before annealing at 550 °C in N_2 atmosphere for 60 s. Doping with La^{3+} was made at ≈1.6 at% dopant as determined by Rutherford backscattering spectrometry (RBS) analysis. The deposited layers were further characterized by X-ray reflectometry (XRR), grazing-incidence X-ray diffraction (GIXRD), scanning electron microscopy (SEM), energy-dispersive X-ray analysis (EDS), and time-of-flight secondary-ion mass spectrometry (TOFSIMS). As such, the physical characteristics, namely, thickness, crystallization behavior, grain morphology, and chemical elements distribution, were evaluated. Polarization–electric field (*P*–*E*) plots and the corresponding current–electric field (*I*–*E*) characteristics of the MFM capacitors were measured at 10 kHz and room temperature. Remanent polarization (P_r^+ and P_r^-) was calculated from the *P*–*E* hysteresis loop at $E = 0$. Double remanent polarization ($2P_r$) was calculated as the sum of absolute values of positive and negative remanant polarizations. Fatigue measurements were carried out with bipolar pulses with rise, fall, and flat times of 200 ns at 250 kHz or at 833 kHz.

Acknowledgements

This work is performed under Imec's Industrial affiliation program on ferroelectrics.

Conflict of Interest

The authors declare no conflict of interest.

Data Availability Statement

Research data are not shared.

Keywords

endurance, ferroelectric random-access memory, ferroelectricity, hafnium zirconate, lanthanum, polarization, ZrO_2

Received: January 15, 2021
Revised: February 9, 2021
Published online:

[1] M. H. Park, H. J. Kim, Y. J. Kim, Y. H. Lee, T. Moon, K. D. Kim, S. D. Hyun, F. Fengler, U. Schroeder, C. S. Hwang, *ACS Appl. Mater. Interfaces* **2016**, *8*, 15466.
[2] S. Shibayama, T. Nishimura, S. Migita, A. Toriumi, *J. Appl. Phys.* **2018**, *124*, 184101.
[3] M. H. Park, H. J. Kim, Y. J. Kim, W. Lee, T. Moon, C. S. Hwang, *Appl. Phys. Lett.* **2013**, *102*, 242905.
[4] A. G. Chernikova, M. G. Kozodaev, D. V. Negrov, E. V. Korostylev, M. H. Park, U. Schroeder, C. S. Hwang, A. M. Markeev, *ACS Appl. Mater. Interfaces* **2018**, *10*, 2701.
[5] M. G. Kozodaev, A. G. Chernikova, E. V. Korostylev, M. H. Park, R. R. Khakimov, C. S. Hwang, A. M. Markeev, *J. Appl. Phys.* **2019**, *125*, 034101.
[6] S. S. Fields, S. W. Smith, P. J. Ryan, S. T. Jaszewski, I. A. Brummel, A. Salanova, G. Esteves, S. L. Wolfley, M. D. Henry, P. S. Davids, J. F. Ihlefeld, *ACS Appl. Mater. Interfaces* **2020**, *12*, 26577.
[7] T. Onaya, T. Nabatame, M. Inoue, Y. C. Jung, H. Hernandez-Arriaga, J. Mohan, H. S. Kim, N. Sawamoto, T. Nagata, J. Kim, A. Ogura, *ECS Trans.* **2020**, *98*, 63.
[8] T. Onaya, T. Nabatame, N. Sawamoto, A. Ohi, N. Ikeda, T. Chikyow, A. Ogura, *Appl. Phys. Express* **2017**, *10*, 081501.
[9] T. Onaya, T. Nabatame, M. Inoue, Y. C. Jung, H. Hernandez-Arriaga, J. Mohan, H. S. Kim, N. Sawamoto, T. Nagata, J. Kim, A. Ogura, *Appl. Phys. Lett.* **2020**, *117*, 232902.
[10] T. Onaya, T. Nabatame, N. Sawamoto, A. Ohi, N. Ikeda, T. Nagata, A. Ogura, *APL Mater.* **2019**, *7*, 061107.
[11] L. Luterotti, P. Scardi, *J. Appl. Cryst.* **1990**, *23*, 246.
[12] V. Mukundan, S. Consiglio, D. H. Trioso, K. Tapily, S. Schujman, C. Mart, T. Kampfe, W. Weinreich, J. Jordan-Sweet, R. D. Clark, G. J. Leusink, A. C. Diebold, *Appl. Phys. Lett.* **2020**, *117*, 262905.
[13] J. Müller, T. S. Böscke, U. Schröder, S. Mueller, D. Bräuhaus, U. Böttger, L. Frey, T. Mikolajick, *Nano Lett.* **2012**, *12*, 4318.
[14] P. D. Lomenzo, Q. Takmeel, C. Zhou, C. M. Fancher, E. Lambers, N. G. Rudawski, J. L. Jones, S. Moghaddam, T. Nishida, *J. Appl. Phys.* **2015**, *117*, 134105.
[15] C. Künneth, R. Materlik, A. Kersch, *J. Appl. Phys.* **2017**, *121*, 205304.
[16] T. Schenk, U. Schroeder, M. Pesic, M. Popovici, Y. V. Pershin, T. Mikolajick, *ACS Appl. Mater. Interfaces* **2014**, *6*, 19744.
[17] M. Pesic, M. Hoffmann, C. Richter, T. Mikolajick, U. Schroeder, *Adv. Funct. Mater.* **2016**, *26*, 7486.
[18] F. Huang, X. Chen, X. Liang, J. Qin, Y. Zhang, T. X. Huang, Z. Wang, B. Peng, P. H. Zhou, H. P. Lu, L. Zhang, L. J. Deng, M. Liu, Q. Liu, H. Tian, L. Bi, *Phys. Chem. Chem. Phys.* **2017**, *19*, 3486.
[19] P. Jiang, Q. Luo, X. Xu, T. Gong, P. Yuan, Y. Wang, Z. Gao, W. Wei, L. Tai, H. Lv, *Adv. Electron. Mater.* **2021**, *7*, 2000728.
[20] H. Chen, L. Tang, L. Liu, Y. Chen, H. Luo, X. Yuan, D. Zhang, *Materialia* **2020**, *14*, 100919.
[21] A. Chouprik, M. Spiridonov, S. Zarubin, R. Kirtaev, V. Mikheev, Y. Lebendinskii, S. Zakharchenko, D. Negrov, *ACS Appl. Electron. Mater.* **2019**, *1*, 275.
[22] T. Song, R. Bachelet, G. Saint-Girons, R. Solanas, I. Fina, F. Sanchez *ACS Appl. Electron. Mater.* **2020**, *2*, 3221.
[23] F. Mehmood, M. Hoffmann, P. D. Lomenzo, C. Richter, M. Materano, T. Mikolajick, U. Schroeder, *Adv. Mater. Interfaces* **2019**, *6*, 1901180.

